

## Optimization of the W7-X pumping system

D. Sharma, Y. Feng, F. Sardei, H. Grote, P. Grigull, H. Renner  
*Max-Planck-Institut für Plasmaphysik, IPP-Euratom Association*  
*Teilinstitut Greifswald, Wendelsteinstr. 1, D-17491 Greifswald, Germany*

### 1 Introduction

Analysis of neutral particle transport is of importance for the successful steady-state divertor operation proposed for the stellarator W7-X. In addition to the range of magnetic configurations and the incident energy flux, the divertor design for W7-X is also being optimized for an additional control over the plasma using the particle sources in the divertor region [1]. The present work aims at characterizing the plasma and neutral particle transport processes in the plasma edge region using the 3D Monte Carlo code EMC3-EIRENE [2, 3]. The self-consistent analysis of plasma and neutral transport is done in order to optimize the divertor operation by effectively controlling the exposure of neutral particles in subdivertor volume to the edge plasma. The study involves simulation of the plasma transport to determine the density, temperature and flow velocity profiles in the plasma edge region of W7-X. The neutral transport is then simulated self-consistently by allowing the neutral particle concentration to build up in the divertor chamber and effectively controlling its interaction with the edge plasma through a pumping gap which is varied.

The code EMC3-EIRENE, recently upgraded to incorporate arbitrary magnetic structures, uses a 3D grid for sampling the plasma and neutral parameters. The significantly large volume of W7-X plasma requires a proportionally large number of grid points for sampling plasma parameters since the required resolution is fixed by the scale lengths which are largely independent of the total plasma volume. The 3D divertor geometry also adds to the complexity of the analysis and requires a carefully chosen grid structure.

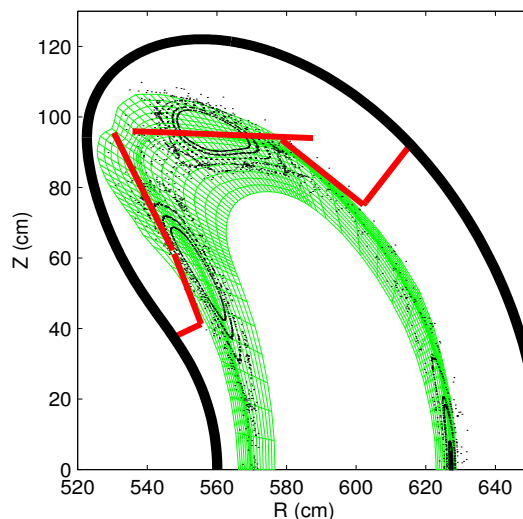


Figure 1: The magnetic configuration and the computational mesh for W7-X.

## 2 Simulation procedure

The 3D mesh used for simulation represents a set of flux tubes which are subdivided into toroidal cells to score particles. A finer cell size is required to resolve the region close to the divertor surfaces, where the neutral source is located and plasma parameters have the largest variation. This resolution is maintained on all toroidal locations on the 3D helical surface of the divertor plates. Apart from the finer geometric grid a coarser physical grid is used for defining physical variables. A 3 % subset of the geometric grid is plotted in the up-down symmetric bean shaped cross-section (Fig. 1).

## 3 Plasma transport in W7-X

The first application of EMC3-EIRENE for the W7-X geometry is implemented. The plasma profiles are simulated self-consistently using an iterative procedure for the magnetic field configuration with  $\iota = 5/5$  and  $\langle \beta \rangle = 4\%$ . As shown in Fig. 1, the magnetic

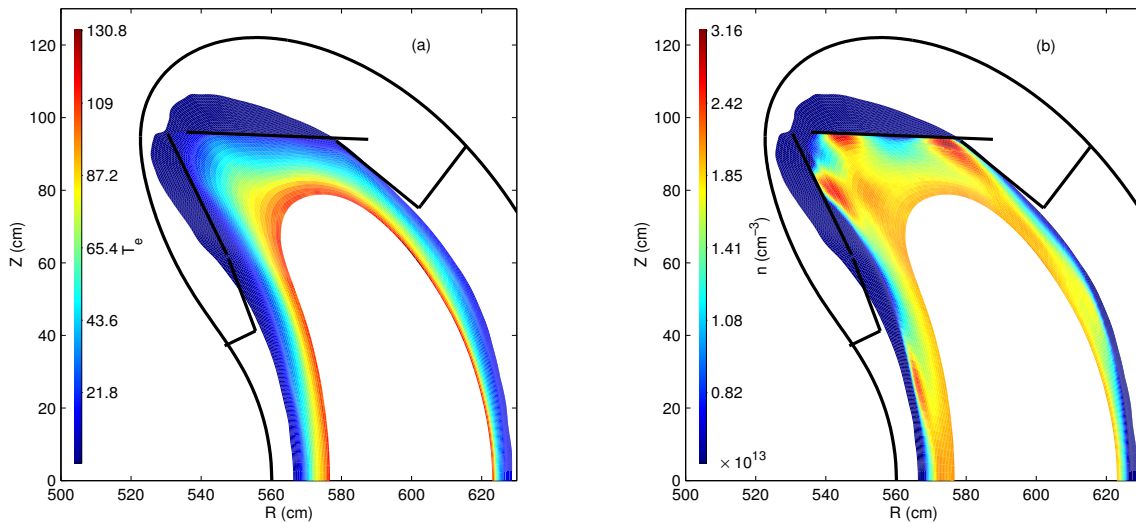


Figure 2: The electron temperature  $T_e$  (eV) (a) and plasma density  $n$  (b).

configuration is characterized by a combination of regular flux surfaces, islands and ergodic structures in the region of separatrix. For the present study a constant influx of energy entering the SOL region, 5 MW, is used from the core region. The edge plasma density is fixed by the choice of total plasma flow to the targets while the volume sources are used as generated by EIRENE code. At the targets the Bohm boundary condition is used. The resulting distributions of plasma density and temperature are shown in Fig. 2. The deposition channels to the target plates could be clearly identified as they follow

the island structure. The volume sources are seen to peak on the the target surfaces with maximum value on the horizontal target plate close to the  $\phi = 0$  plane (where  $\phi$  is the toroidal angle). The deposition of particle and energy flux on the target element could also be obtained and used for the neutral particle calculations presented in Section 4.

## 4 Divertor processes and neutral particle analysis

The planned divertor unit consists of ten discontinuous sets of vertical and horizontal target plates installed up down symmetrically. Each set cuts two islands at different poloidal locations. In the present study we characterize the divertor performance and subdivertor neutral density for the steady-state operating conditions. Also the performance of pumping system is characterized with respect to divertor geometry where the estimation of achievable pumping speeds could be obtained over a range of pumping system efficiency. The self-consistently generated recycling neutrals are used and the neutral density in the divertor chamber is analyzed by varying the divertor pumping gap, thereby controlling the exposure

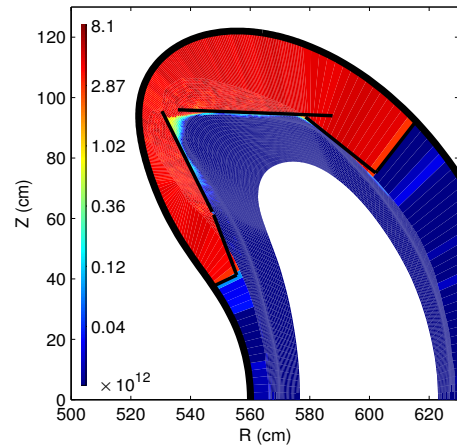


Figure 3:  $H_2$  density distribution ( $\text{cm}^{-3}$ ), for  $A = A_0$ .

of neutrals to the plasma. The average neutral density in the divertor chambers was calculated for a range of divertor openings in order to validate the current divertor designs. The neutral particle analysis was carried out with a plasma background calculated with the current divertor geometry and pumping switched off. This approximation is reasonable since the neutral backflow from the divertor chamber to plasma is small compared to the recycling flux. The subdivertor molecular density plotted in Fig. 3 corresponds to the currently chosen pumping gap configurations at  $\phi = 0$  plane. The detailed dependence of the average molecular density on the divertor opening is plotted in Fig. 4 with varying pumping efficiency  $\alpha$  (ratio of absorbed and incident flux on pumping area). Here the pumping gap area  $A$  is normalized to that in the current divertor design  $A_0$ .

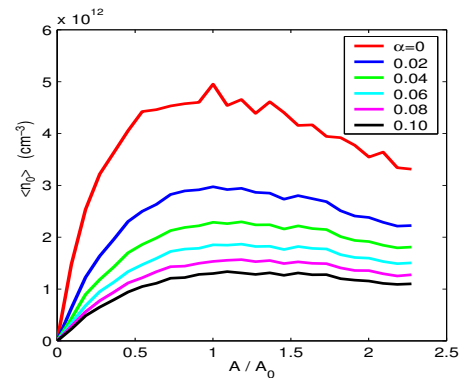


Figure 4: Dependence of averaged molecule density  $\langle n_0 \rangle$  ( $\text{cm}^{-3}$ ) on pumping gap  $A$  and efficiency  $\alpha$  at  $\phi = 0$ .

of neutrals to the plasma. Here the pumping gap area  $A$  is normalized to that in the current divertor design  $A_0$ .

It could be seen that beginning from zero the neutral density grows rapidly at smaller values of the gap, although the growth stops owing to a dominant backflow of the neutrals into the plasma at a critical gap area. A larger opening results in a larger sink of neutrals in the plasma and causes reduction in the subdivertor neutral density. It could be noted that the maximum subdivertor neutral density occurs at  $A = A_0$  representing an optimum pumping efficiency at the current design specifications, for this case an averaged neutral compression ratio of  $1.7 \times 10^2$  is estimated for  $H_2$  at a representative cross-section ( $\phi = 0$ ) with pumping switched off. The achievable pumping speeds could be estimated for a range of pumping efficiency and plotted in Fig 5. For the proposed locations and geometrical specifications of the pumping mechanism. The total pumping area of cryo-pump unit was represented by additional absorbing surfaces located in the divertor chamber. The absorption coefficient  $\alpha$  is varied from 2 to 10 percent of the incident flux which yields an optimum total pumping speed of  $3.5 \times 10^{21} \text{ s}^{-1}$  at an average neutral density of  $1.0 \times 10^{12} \text{ cm}^{-3}$  and an average pumping efficiency of 10 %, enabling a higher NBI input power and improved particle exhaust. Better results are expected with enhanced pumping efficiency, up to 20 %, of the cryo-pumps.

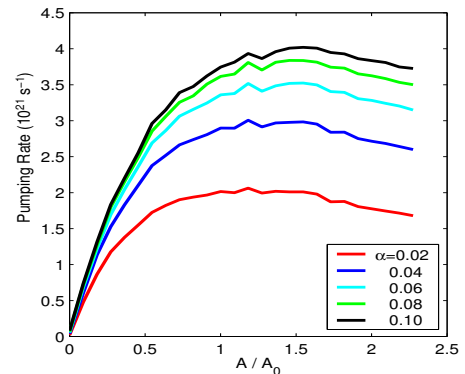


Figure 5: Dependence of  $H_2$  pumping speed on pumping efficiency  $\alpha$ .

## 5 Conclusions

The 3D code EMC3-EIRENE was implemented for W7-X and first self-consistent results were obtained for plasma and neutrals. One of the major tasks has been to optimize the grid structure according to required resolution. The dependence of neutral particle behavior on the pumping efficiency and the pumping gap is investigated. The characterization and validation of current design specifications is done for the optimum operating conditions.

## References

- [1] H. Renner et al., Nucl. Fusion., Vol. 40, No. 60, (2000) 1083.
- [2] Y Feng et al., J. Nucl. Mater., 241-243 (1997) 930.
- [3] Y Feng et al., J. Nucl. Mater., 266-269 (1999) 812.